TISSUE ENGINEERING: Part A
Volume 26, Numbers 5 and 6, 2020

DOI: 10.1089/ten.tea.2019.0181

termis
Tissue Engineering
& Regenerative Medicine
International Society

ORIGINAL ARTICLE

In Vivo Evaluation of Three-Dimensional Printed, Keratin-Based Hydrogels in a Porcine Thermal Burn Model

Javier Navarro, PhD,[1,2] Ryan M. Clohessy, PhD,[3] Robert C. Holder, PhD,[3] Alexis R. Gabard, PhD,[3] Gregory J. Herendeen, PhD,[3] Robert J. Christy, MD,[4] Luke R. Burnett, PhD,[3] and John P. Fisher, PhD[1,2]

Keratin is a natural material that can be derived from the cortex of human hair. Our group had previously presented a method for the printed, sequential production of three-dimensional (3D) keratin scaffolds. Using a riboflavin–sodium persulfate–hydroquinone (initiator–catalyst–inhibitor) photosensitive solution, we produced 3D keratin-based constructs through ultraviolet crosslinking in a lithography-based 3D printer. In this study, we have used this bioink to produce a keratin-based construct that is capable of delivering small molecules, providing an environment conducive to healing of dermal burn wounds *in vivo*, and maintaining stability in customized packaging. We characterized the effects of manufacturing steps, such as lyophilization and gamma irradiation sterilization on the properties of 3D printed keratin scaffolds prepared for *in vivo* testing. Keratin hydrogels are viable for the uptake and release of contracture-inhibiting Halofuginone, a collagen synthesis inhibitor that has been shown to decrease collagen synthesis in fibrosis cases. This small-molecule delivery provides a mechanism to reduce scarring of severe burn wounds *in vitro*. *In vivo* data show that the Halofuginone-laden printed keratin is noninferior to other similar approaches reported in literature. This is indicative that the use of 3D printed keratin is not inhibiting the healing processes, and the inclusion of Halofuginone induces a more organized dermal healing after a burn; in other words, this treatment is slower but improves healing. These studies are indicative of the potential of Halofuginone-laden keratin dressings in dermal wound healing. We aim to keep increasing the complexity of the 3D printed constructs toward the production of complex scaffolds for the treatment and topographical reconstruction of severe burn wounds to the face.

Keywords: keratin, biomaterial, hydrogel, burns, animal model, 3D printing

Impact Statement

Keratin-based photosensitive bioink can be used to three-dimensionally (3D) print complex scaffolds for the topical treatment of dermal burn wounds. We have developed reproducible protocols that allow us to 3D print large volumes of keratin-based hydrogels, and we now have a better understanding of how 3D printed geometrical features, crosslinking properties, or mass are altered due to the manufacturing processes. The printed hydrogels improved healing parameters *in vivo* on a porcine thermal burn model, indicative of the potential of the scaffolds for the regeneration of complex dermal wounds. Overall, our approach elucidates on physiological and topographical 3D healing of burn wounds.

Introduction

In the treatment of dermal burn wounds, the severity of the injury can increase if the burn is not properly managed.[1] An optimal dressing for initial burn injuries would absorb exudates and maintain a moist, clean environment while preventing the development of additional necrotic tissue, thus preventing further burn wound conversion, scarring, and minimizing the area in need of medical intervention. Once the initial injury has been addressed and surgical intervention can be initiated, this same dressing should be able to continue to provide an environment conducive to

[1]Fischell Department of Bioengineering, University of Maryland, College Park, Maryland.
[2]Center for Engineering Complex Tissue, University of Maryland, College Park, Maryland.
[3]KeraNetics, LLC, Winston-Salem, North Carolina.
[4]U.S. Army Institute of Surgical Research, Combat Trauma and Burn Injury Research, San Antonio, Texas.

healing and discourage scar formation and contracture. Ideally, this dressing would be customized to the individual's anatomy to provide a matrix that encourages a return to an esthetically acceptable structure.

Protein-based materials have become attractive natural polymer options for tissue engineering and regenerative medicine (TERM), including dermal applications and the optimization of dressings.[2,3] Proteins provide three-dimensional (3D) structures that facilitate cell attachment, proliferation, and migration.[4–7] Of note, keratin-based materials are a viable option for scaffold development due to their biocompatibility, structural characteristics, and abundance as a renewable resource.[2,8]

Keratins are a family of insoluble proteins found in epithelial tissues that can be obtained from epidermal structures such as feathers, hooves, wool, and human hair.[2,9] They exhibit the ability to self-assemble or be crosslinked to form porous, fibrous hydrogel scaffolds.[2,8,10–12] Keratin-based biomaterials have been used in nerve, muscle, skin, and bone TERM applications.[9,13–22] Keratins also contain motifs important for cellular attachment, such as leucine–aspartic acid–valine (LDV) and glutamic acid–aspartic acid–serine (EDS) residues.[23–25] Keratins have been shown to promote cellular attachment of adipose-derived stem cells,[26] osteoblasts,[9,27] hepatocytes,[28] neural cells,[13] and fibroblasts.[29] Furthermore, keratin biomaterials can be used as tunable vehicles for delivery of small molecules or cells to treat dermal wounds.

Keratin-based biomaterials have been successfully used for the delivery of growth factors (e.g., insulin-like growth factor-1, basic fibroblast growth factor [bFGF]),[30,31] progenitor cells (e.g., skeletal muscle myoblasts),[16] and antimicrobial agents (ciprofloxacin),[32] among other molecules. In this study, we studied Halofuginone-laden keratin scaffolds for the *in vivo* treatment of burn, particularly the development of an individualized keratin-based dressing capable of encouraging quick wound healing with the release of Halofuginone. Halofuginone was selected based on its effectiveness in preventing abnormal fibrillar collagen accumulation in pathologies associated with fibrosis and wound contracture.[33–36] Halofuginone is an FDA-approved collagen I synthesis inhibitor that decreases collagen synthesis by inhibiting transforming growth factor beta-dependent Smad3 phosphorylation.[35]

Keratin can be extracted from the cortex of human hair using reductive or oxidative chemistry.[37] Reduced keratin can self-assemble due to the formation of disulfide bonds between cysteine amino acids in the protein chain; oxidation, on the other hand, causes capping of the cysteine groups and greatly decreases the self-assembling capacity.[9] We previously reported the formulation of a keratin-based bioink for 3D printing by incorporating oxidized keratin into a photosensitive initiator–catalyst–inhibitor (riboflavin–sodium persulfate[SPS]–hydroquinone) solution.[8,38,39] Ultraviolet (UV) light was used to induce dityrosine crosslinking between keratin chains.[8,38,39] Our previous studies indicate that a keratin scaffold can be 3D printed and that this construct could be used to efficiently uptake and release entrained solutions.[8]

The work in this study seeks to expand these findings. We aim to produce a keratin-based scaffold that is capable of (1) releasing a drug such as Halofuginone, (2) providing an environment conducive to *in vivo* healing of burn wounds, and (3) maintaining stability in customized packaging. We hypothesized that a Halofuginone-laden keratin scaffold, printed to meet the wound dimensional needs, would slowly degrade on the skin, providing a moist environment, absorbing exudate, and delivering the collagen-inhibiting drug Halofuginone to reduce scarring while negating the need for painful wound dressing changes. We first assessed the viability of our bioink for the production of scaffolds for topical use on wounds, particularly the retention of geometrical features after the manufacturing processes. Second, we confirmed the viability of our 3D printed keratin-based hydrogel for prevention of burn contracture *in vitro* using a collagen gel contracture assay. Third, the efficacy of Halofuginone-loaded scaffolds on healing dermal wounds was assessed *in vivo* using a porcine burn model, studying parameters such as collagen order, regrowth of dermal appendages, and lack of hyperkeratosis or hyperplasia.

Materials and Methods

Keratin extraction and bioink preparation

Keratin extraction was conducted following the protocol adapted from de Guzman *et al.*[40] Briefly, human hair was oxidized in excess 2% peracetic acid (Sigma-Aldrich Co., St. Louis, MO) for 10 h at 37°C on an orbital shaker. The treated hair was rinsed sequentially with water, excess 100 mM Tris base, and 40-fold excess of ultrapure water. Between rinses the solutions were strained through 500-μm sieves and the liquids recovered and centrifuged to recover insoluble particles. The resultant filtrates were purified using filtration and dialysis. The crude extract was concentrated (pH 7.4), lyophilized, and ground into powder form. The keratin-based bioink was then prepared as detailed in our previous publications.[8,38,39] Briefly, lyophilized keratin was dissolved in phosphate-buffered saline (PBS) at a concentration of 4% wt/vol. The keratin solution was combined with a photosensitive initiator-catalyst-inhibitor solution using a 4:1 ratio. This photosensitive solution was made of 1 mM riboflavin (Sigma-Aldrich), 200 mM SPS (Sigma-Aldrich), and 0.001% wt/vol hydroquinone (Sigma-Aldrich). After thorough mixing the bioink is curable under UV light.

Three-dimensional printing: continuous digital light processing

Keratin-based bioink was used to 3D print keratin hydrogels on a lithography-based EnvisionTEC Perfactory 4 DLP printer (EnvisionTEC, Inc., Dearborn, MI). UV exposure time was fixed to 240 s per 100 μm layer, with intensity of 350–375 mW/dm^2. Samples were printed with circular cross-section, 2 mm thick, with either 15 (characterization and contracture assays) or 30 mm (animal burn model) diameter (Fig. 1A, B). Samples for rehydration and soluble fraction (sol fraction) studies had additional thickness groups. Printed samples could either be rinsed in PBS and stored at 4°C, or loaded into custom 3D printed cases and frozen at −80°C. The cases were printed on the Perfactory printer using EShell 300 resin (EnvisionTEC) (Fig. 1D) to hold the scaffolds during freezing, lyophilization, sterilization, and transport. When appropriate, samples were lyophilized in a FreeZone Lyophilizer (LABCONCO, Kansas City, MO) at a 0.018 mBar vacuum and −48°C for 24 h, after which they were sterilized under gamma radiation.

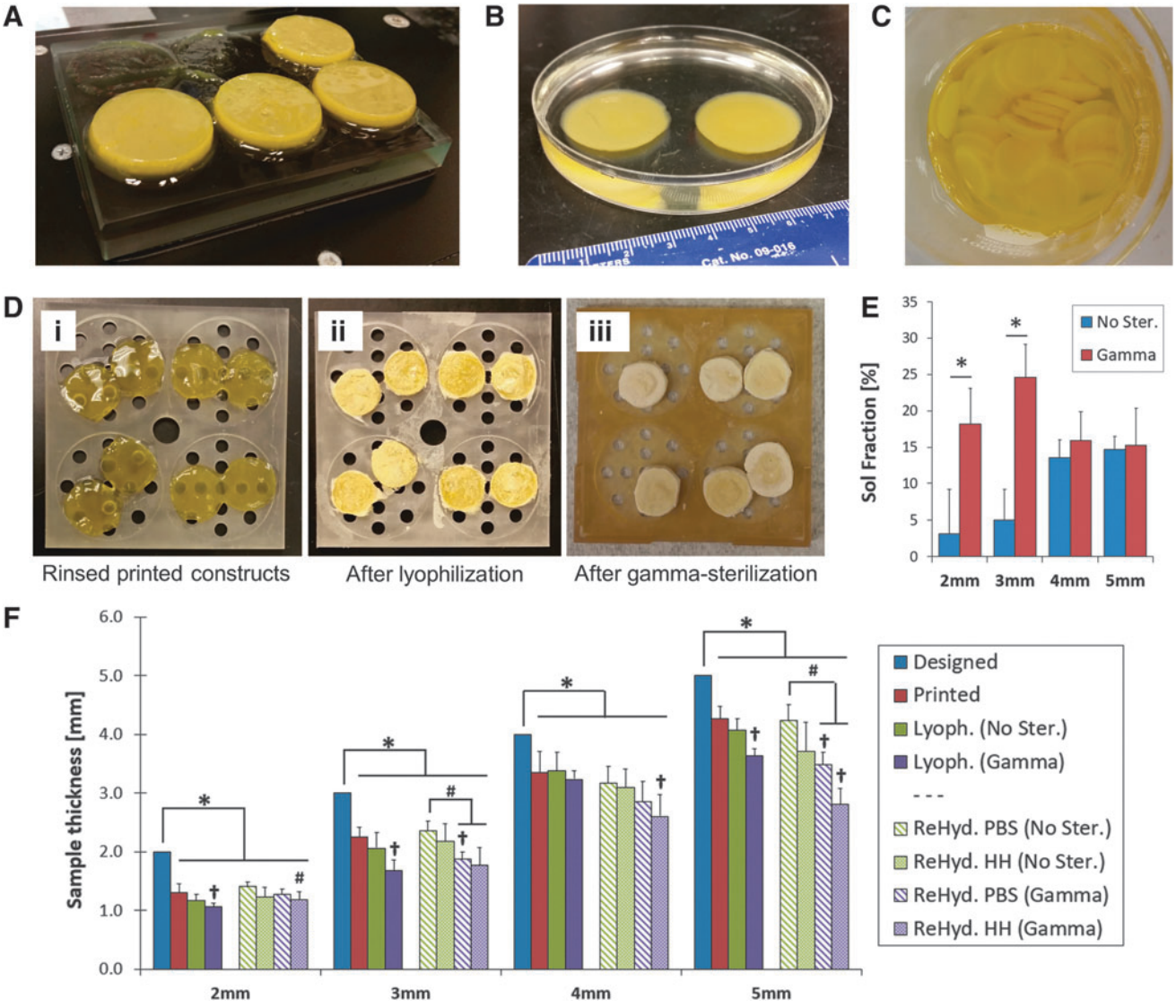

FIG. 1. Three-dimensional printed keratin-based scaffolds for *in vitro* and *in vivo* assessments. **(A)** Four percent wt/vol scaffolds 3D printed on a lithography-based EnvisionTEC Perfactory 4 DLP printer. **(B)** Crosslinked samples are stable and retain their printed dimensions after swelling in PBS. **(C)** The protocol yields consistent batches of hydrogels with reproducible dimensions for standardized testing. **(D)** Three-dimensional printed cases were produced to hold the hydrogels throughout the manufacturing process. The cases held samples during **(i)** rinsing; **(ii)** freezing at −80°C and lyophilization; and **(iii)** sterilization with gamma irradiation. **(E)** End-point sol fraction reveals significant effects of gamma irradiation on mass loss of thinner constructs. The 2- and 3-mm thick samples have lower sol fraction before sterilization than 4- and 5-mm thick ones, but gamma irradiation increases the amount of soluble components at the end-point; statistical significance: *difference between nonsterilized and gamma irradiated sample (*t*-test, $p < 0.05$). **(F)** Sterilization and rehydration media have significant effects on the thickness of the hydrogel endproducts. All printed scaffolds differ from the designed constructs and lyophilization does not significantly further reduce the thickness, but gamma irradiation does. Rehydration in HH or PBS cannot fully restore the dimensions, resulting in thickness loss over 2 mm. Statistical significance: *mean thickness differs from the *Designed* value (*t*-test, $p < 0.05$); †thickness differs from the *Printed* value (ANOVA per thickness group, $p < 0.05$); #thickness differs from the *ReHyd. PBS (No Ster.)* value (ANOVA per thickness group, $p < 0.05$). Sample size $n = 12$ for all studies. 3D, three-dimensional; ANOVA, analysis of variance; HH, Halofuginone hydration; PBS, phosphate-buffered saline.

Rehydration and sol fraction of keratin hydrogels

The effects of the manufacturing process, particularly lyophilization and rehydration, on the dimensions of 3D printed keratin hydrogels were assessed. Samples with 15 mm diameter circular cross-section were printed with 2, 3, 4, or 5-mm thickness (designed values, $n = 12$). Mass and thickness of the samples were recorded (unrinsed values), after which they were moved into excess PBS for 48 h to rinse out uncrosslinked residues. Mass and thickness of the samples were measured (printed values) and samples were then frozen at −80°C overnight followed by 24 h lyophilization. After, mass and thickness of the samples were recorded again (lyophilized values). Half of the samples were

left unsterilized, and the remaining were sterilized under gamma irradiation. Samples from all groups were then rehydrated in either PBS or a Halofuginone hydration (HH) methanol solution (25% methanol [Fisher Scientific, Hampton, NH], 25% milliQ water, 50% PBS) for 1 h, after which mass and thickness of the samples were measured (rehydration values). All samples were then moved to excess PBS for 5 days, after which the samples were lyophilized again, and mass and thickness were recorded for the last time (final rinsed values). The sol fraction (%) of the sample was calculated as the difference between the unrinsed mass and the final rinsed mass, over the total mass ($n = 12$).

In vitro *collagen gel contracture assay*

Impact on fibroblast-mediated contracture was examined using a collagen gel contracture assay. A collagen gel working solution (bovine type I collagen at 3.0 mg/mL) was prepared according to the manufacturer's protocol (Cell BioLabs, San Diego, CA), and mixed with 500,000 cells/mL suspension of adult normal human dermal fibroblasts (HDF; ATCC, Manassas, VA) in a ratio of 4:1 (collagen:cells). Samples of 500 μL of the collagen/cell mixture were plated in 24-well plates and incubated (37°C). After 1 h, 1.5 mL of media were added to each well. The following day, collagen gels were released from the walls and floor of the well using a 20 μL pipette tip. Then, Falcon transwell inserts with a pore size of 8 μm were placed in each well over the collagen gels, carrying the keratin-based hydrogels to assess 3D printed keratin with or without Halofuginone. Overall, the groups studied were: unseeded collagen without hydrogel treatment (no cells, negative control); HDF-seeded collagen without hydrogel treatment (HDF cells only, positive control); HDF-seeded collagen with keratin hydrogel treatment (3D printed keratin); and HDF-seeded collagen with Halofuginone-laden keratin hydrogel treatment (3D printed keratin + Halofuginone). Digital images were taken from a fixed position with fixed ruler in the field of view at time 0 (gel release), 12, and 24 h.

In vivo *porcine burn model*

In vivo evaluation of the 3D printed keratin constructs was conducted using a 3 cm red Duroc porcine circular burn model as approved by the Institutional Animal Care and Use Committees (IACUC) at the U.S. Army Institute of Surgical Research and at the University of Maryland. A total of 24 wound areas were marked on each pig (two rows of 6 wounds on each side of the midline, at least 3 cm from the spine line, on two animals). Each area was separated from other wound areas by 3 cm to prevent site-to-site influence. The skin was tattooed over these markings using an electric tattoo machine (Spaulding and Rogers, Voorheesville, NY) to provide guidance as to where to take biopsies postinjury. Pigs were sedated with an injection of acepromazine (0.5–1.5 mg/kg) and ketamine (10–25 mg/kg,) into the clavotrapezius muscle just behind the ear. During the procedure, a nose cone attached to the anesthesia machine was used to deliver isoflurane (3–4%) with an oxygen flow rate of 3–4 L/min. A 0.9% NaCl solution was delivered intravenously into an ear vein to maintain hydration. The animals were intubated, and isoflurane was maintained at 2% throughout the procedure. To perform the burn, brass cylinders (3 cm diameter) were heated in a dry bath incubator to 100°C, after which the external contacting surface of the cylinder was placed on the skin of the pig, as performed previously.[17] The brass cylinder was held in contact with the skin for 17 s to produce a deep partial-thickness burn. Before bandaging, the burn wounds were allowed to cool and pictures were taken. Afterward, Tegaderm™ dressing (3M, Maplewood, MN) was placed over the wound, followed by nonadherent TELFA gauze taped into place with Elastikon surgical tape. A layer of antibiotic Ioban was then used to cover the entire dorsum/flank of the animal.

On postburn day 3, the animal was again anesthetized, the dressing was removed, and the following treatments applied: Group 1 (3D Halo), a 3D printed lyophilized keratin-based hydrogel loaded with 225 μg/mL Halofuginone; Group 2 (keratin cream), a proprietary formulation for a 5% nonlyophilized keratin topical solution supplemented with emollients, emulsifiers, and humectants to provide a creamy consistency; Group 3 (no treatment), negative control; and Group 4 (3D Keratin unloaded), a 3D printed lyophilized unloaded keratin-based hydrogel. Treatments were bandaged as before. At either 30 or 70 days postinjury, bandages were removed, wounds observed, and select wounds biopsied ($n = 6$ per group, per time point).

Histomorphologic wound evaluation

On days 30 and 70, animals were anesthetized as detailed above and burns were assessed using a histomorphologic scale to quantify cutaneous scarring, as described by Singer *et al.*[41] Biopsy samples were collected to ensure that the excised biopsy spanned the burn site, strips 0.5 cm in width $\times$ 4 cm in length were obtained through the middle of the burned tissue, extending beyond the margins (normal skin to normal skin). Samples were placed in 10% formalin for at least 48 h before processing. Samples were embedded in paraffin, cut into 6 μm-thick sections, and mounted onto glass slides. Slides were stained with Hematoxylin and Eosin (H&E), Masson's Trichrome, alpha smooth muscle actin, and Picrosirius Red to monitor structural changes of the tissue over time, following regular protocols.

Images were semiquantitatively scored in a blind manner by a veterinary pathologist using a scale for the following categories: presence or absence of (1) epidermal hyperkeratosis, (2) epidermal hyperplasia, (3) inflammation, (4) vascular proliferation at late-stage wound healing, (5) collagen orientation, (6) hair follicles, (7) apocrine glands, and (8) smooth muscle. Each parameter examined was assigned a score of +1 for a normal finding; otherwise, a score of 0 was given. The presence of normal collagen was assigned a maximum score of +3, followed by a decreasing score of +2 to 0 given to progressively deeper scar: +2 involving the papillary dermis, +1 for upper half of reticular dermis, and 0 for upper and lower half of the reticular dermis. The total histology score was determined by adding all individual scores. The best possible outcome was a score of 10, equivalent to normal tissue with no residual scarring. A score of 0 was equivalent to a deep scar involving all layers of skin. Points are given for the findings as described in Table 1.

Statistics

Statistics for quantitative tests were performed using analysis of variance (ANOVA) and Tukey's multiple pairwise

Table 1. Scoring Parameters for Wound Healing *In Vivo*

Parameter examined	*Scoring*	*Parameter examined*	*Scoring*
Hyperkeratosis	Absent (1) Present (0)	Smooth muscle	Absent (0) Present (1)
Epidermal hyperplasia	Absent (1) Present (0)	Collagen orientation	Normal (3) Abnormal Pap. dermis (2) Abnormal upper reticular dermis (1) Abnormal upper/lower reticular dermis (0)
Hair follicles	Absent (0) Present (1)	Active chronic inflammation	Absent (1) Present (0)
Apocrine glands	Absent (0) Present (1)	Vascular proliferation	Absent (1) Present (0)

comparisons (significance using $p<0.05$). Differences between individual groups and references were assessed with two-sample *t*-test for the mean. For the wound healing data, statistical analysis was conducted using GraphPad Prism 7.0 for Windows (La Jolla, CA) with data expressed as the mean ± standard of error. Histological scores were considered nonparametric data; a nonparametric, two-way ANOVA and *t*-test using Holm–Sidak Method were used to study these sets (significance using $p<0.05$).

Results and Discussion

The goal of this work was to assess the viability of a 3D printed keratin-based construct that is capable of the *in vivo* delivery of Halofuginone for the treatment of dermal burn wounds. Oxidized keratin has been successfully implemented into a UV photosensitive bioink and 3D printed on a lithography-based continuous digital light processing (cDLP) printer using UV light.[8,38,39] This approach yielded biocompatible hydrogels with honeycomb-like structures that allowed high uptake of solutions (PBS or minimum essential media [MEM]) as well as cellular adhesion, proliferation, and migration.[8] Uptake and swelling capacities are characteristics of great interest for drug or growth factor delivery, as well as for cell culturing in TERM applications. Printed scaffolds presented maximum swelling of 1770% and 1580%, with PBS or MEM respectively, exceeding those of casted keratin or gelatin reported in literature.[42–44] The saturation levels were sustained throughout a 5-day observation period without any qualitative changes to the scaffold's dimensions or consistency. Furthermore, we showed that neither the bioink nor the printing process results in significant cytotoxicity, with seeded cells sustaining normal metabolic activity, morphology, and proliferation rates.[8] These results indicated that printed keratin hydrogels are suitable candidates for drug delivery in the treatment of dermal burn wounds.

Alternative crosslinkers such as visible light-induced ruthenium and studies on the adequate loading of the Halofuginone have further confirmed our delivery hypothesis while opening new research questions to study in the future (Supplementary Data and Supplementary Fig. S1). As shown in Figure 1A and B, our 3D printing protocol yields consistent batches of hydrogels with reproducible dimensions. Furthermore, we have a manufacturing protocol that yields large quantities of samples for standardized *in vitro* and *in vivo* testing (Fig. 1C).

Effects of manufacturing processes on the hydrogel mass and dimensions

The geometry of the scaffolds is a key feature in dermal wound healing. The dressing should fit the burn wound site, accommodating the thickness and contours of irregular wounds, to restore the barrier function of skin against irregular water loss or bacterial infection.[45] Even if the geometry is adequately scanned to print a complex dressing, the dimensions must hold throughout the manufacturing process, particularly the sterilization and rehydration steps before application. The custom 3D printed cases (Fig. 1D) used allowed us to track samples along the manufacturing process from production in the laboratory to utilization in the surgery room.

Construct manufacture includes steps that can potentially alter the mass and dimensions of the 3D printed constructs, particularly the steps of rinsing (Fig. 1Di), freezing, lyophilization (Fig. 1Dii), and sterilization (Fig. 1Diii). Tracking mass and dimensions of the samples throughout manufacturing allowed us to assess these alterations quantitatively. As seen in Figure 1E, the soluble fraction at the end of the process indicates significant effects of gamma irradiation on mass loss of thinner constructs. The 2- and 3-mm-thick samples have lower sol fractions without sterilization (3.1% ± 6.4% and 5.0% ± 4.2% respectively) than 4 and 5-mm-thick constructs (13.5% ± 2.5% and 14.6% ± 1.7%, respectively). Gamma irradiation alters the crosslinked networks, particularly for the thinner samples, and results in higher content of soluble components at the sterilized endpoint.

After irradiation, the 2-mm-thick samples had a 478% increase in sol fraction, while the 3 mm samples had a 391% increase. On the other hand, the thick samples only had 17.5% and 3.9% sol fraction increases (4 and 5 mm, respectively). The sol fraction is a measurement of uncrosslinked mass in a hydrogel network. In this case, the intermediate lyophilization and sterilization steps are interfering with the crosslinked network and may produce changes in the shape and mass loss. As samples were crosslinked under the same conditions, particularly exposure time to UV per crosslinked layer, thinner samples initially had a higher crosslinking density, demonstrated with lower sol fraction. Nevertheless, thinner samples are also more vulnerable to gamma penetration, which, as indicated in the sol fraction increase, results in breaking the crosslinked network. Higher sol fraction is indicative of higher mass loss and probably an increased degradation rate *in vivo*.

Sterilization and rehydration also have significant effects on the dimensions of the hydrogels. Thickness was particularly tracked due to the layered nature of the lithography-based 3D printing process. As summarized in Figure 1F, all printed scaffolds are significantly thinner than the original designs. Lyophilization does not significantly further reduce the thickness, but gamma irradiation generally does. Lyophilized samples are sufficient for transportation and sterilization but require a step of rehydration to uptake the Halofuginone before application. Rehydration in methanol HH solution (to solubilize Halofuginone) or PBS was proven to not fully restore the dimensions of the printed samples in all cases, resulting in thickness loss of 2.19 mm in the most extreme case (5 mm, gamma sterilized, rehydrated in HH). The thinner samples, particularly the 2 mm group, were able to rehydrate back to the printed conditions in both HH and PBS. Sterilization with gamma irradiation had significant effects on the samples. In all cases, gamma irradiation resulted in significant reduction of thickness, and those samples then experienced further thinning after rehydration.

The effects of lyophilization and sterilization observed in these studies are in line with our own studies on keratin-based hydrogels and with the reports in literature. In the characterization of the 3D printed keratin we detailed how rinsing in PBS removes uncrosslinked components from the hydrogel, reducing sample mass up to 57%.[38] We observed that freezing and lyophilization cycles induce additional alterations to the crosslinked network. Dimensions of the scaffolds can be generally restored with rehydration in PBS, but the total mass uptake can be irreversibly decreased; this is indicative that swelling assessments, which require a lyophilization step, can be offset due to additional entanglement.[38]

Sterilization methods have been widely studied to determine their effects on hydrogel networks. Gamma radiation has been used before to sterilize keratin-based constructs[15,16,28,31,32]; other methods include UV irradiation, ethanol, or sterile water rinsing.[8,25,38] Gamma radiation is generally accepted as a safe method to reduce bacterial proliferation without inducing cytotoxic side effects.[46,47] On UV-crosslinked poly(ethylene glycol) (PEG) acrylate hydrogels, Escudero-Castellanos *et al.*[47] concluded that gamma irradiation did not affect fibroblast viability and showed significantly lower hemolysis levels (direct human red blood cells incubation) than samples disinfected with 70% ethanol or sterilized in an autoclave.[47] On the other hand, Tyan *et al.*[46] showed that gamma irradiation cleaves peptide linkages and alters collagen-bonded surfaces, suggesting that gamma irradiation of about 10 kGy can significantly degrade the bioactivity of crosslinked collagen surfaces.

Gamma has also been proven to induce dimensional changes due to possible alterations on the crosslinking chemistry. PEG hydrogels sterilized with gamma radiation have higher concentration of radical species when compared with constructs sterilized with ethylene oxide or left unsterilized; gamma-irradiated samples additionally present significant decreases in swelling ratio for all PEG molecular weights and formulations assessed.[48] On natural materials, gamma irradiation has been shown to strongly reduce the bioink viscosity and stability after extrusion of 3D printed alginate and methyl cellulose, significantly reducing printing fidelity. Furthermore, gamma caused significant reduction of methyl cellulose mass over time, indicating that the crosslinked chemistry was altered and eventually released all the components.[49]

Based on the data obtained and literature, it is important to highlight that the manufacturing process of keratin-based hydrogels can result in changes to the 3D printed scaffolds ready for application. Specifically, the steps of lyophilization and rehydration can result in changes in the crosslinked network, loss of mass, and changes in the dimensions of the samples. We want to highlight that the biological effects of the manufacturing process, including the effectiveness of sterilization, of crosslinked keratin hydrogels has been previously characterized and reported.[8] These observations are important for the eventual treatment of complex 3D wounds. Even if the 3D scanning and printing are precise and the bioink is adequate, the manufacturing and preparation of constructs can modify important parameters that could eventually impact healing characteristics such as wound coverage or contraction.

In vitro *contracture of keratin-based hydrogels*

The viability of 3D printed keratin-based hydrogels for prevention of burn contracture was assessed *in vitro* using a collagen gel contracture assay. As illustrated in Figure 2A, the use of 3D printed keratin constructs was always positive to reduce relative contracture compared with a no treatment, HDF-only group. Using unloaded keratin hydrogels saw a contracture reduction close to 53% compared with the HDF-only group. Inclusion of the Halofuginone further reduced contracture, by 83%, compared with the cells-only behavior, coming very close to the no-contracture (no cells) case although still significantly different. Furthermore, the inclusion of Halofuginone significantly reduced contracture compared with the unloaded 3D printed hydrogels.

Contraction of the open wound is necessary to restore the dermal barrier, but uncontrolled contracture due to excessive migration of fibroblasts and disorganized collagen deposition results in higher degrees of scarring.[45,50,51] Increasing wound size and depth reduce wound closure (reapproximation); deep wounds that destroy progenitor fibroblast stem cells rely on re-epithelialization from the wound margins to close, which delays healing and results in higher scarring and contracture.[45] Halofuginone has been proven to prevent abnormal fibrillar collagen accumulation in wound contracture[33–36] by inhibiting collagen I synthase to decrease collagen synthesis,[35] and we have successfully coupled this beneficial feature into our 3D printed constructs.

Scaffolds and dressings, both in research and industry, have attempted to reduce skin wound contracture, particularly collagen-based constructs.[52,53] Commercial products, such as MatriDerm or Hyalograft® C, have been proven to reduce contraction while additionally improving elasticity, epithelialization, and basement membrane formation *in vitro*.[35] Collagen–glycosaminoglycan sponges were used to reduce wound contracture on mice; in this study, the lower concentrations of the 1-ethyl-3-3-dimethylaminopropylcarbodiimide hydrochloride (EDC) crosslinker resulted in better contraction processes, indicating that single components within a regenerative scaffold can greatly impact contracture.[54,55] Similarly, collagen matrices loaded with bFGF were used on a rabbit model and *in vitro* on collagen gels; collagen matrix and bFGF independently promoted reepithelization and reduced contracture, results that were further improved when the two parts were combined as a delivery system.[56]

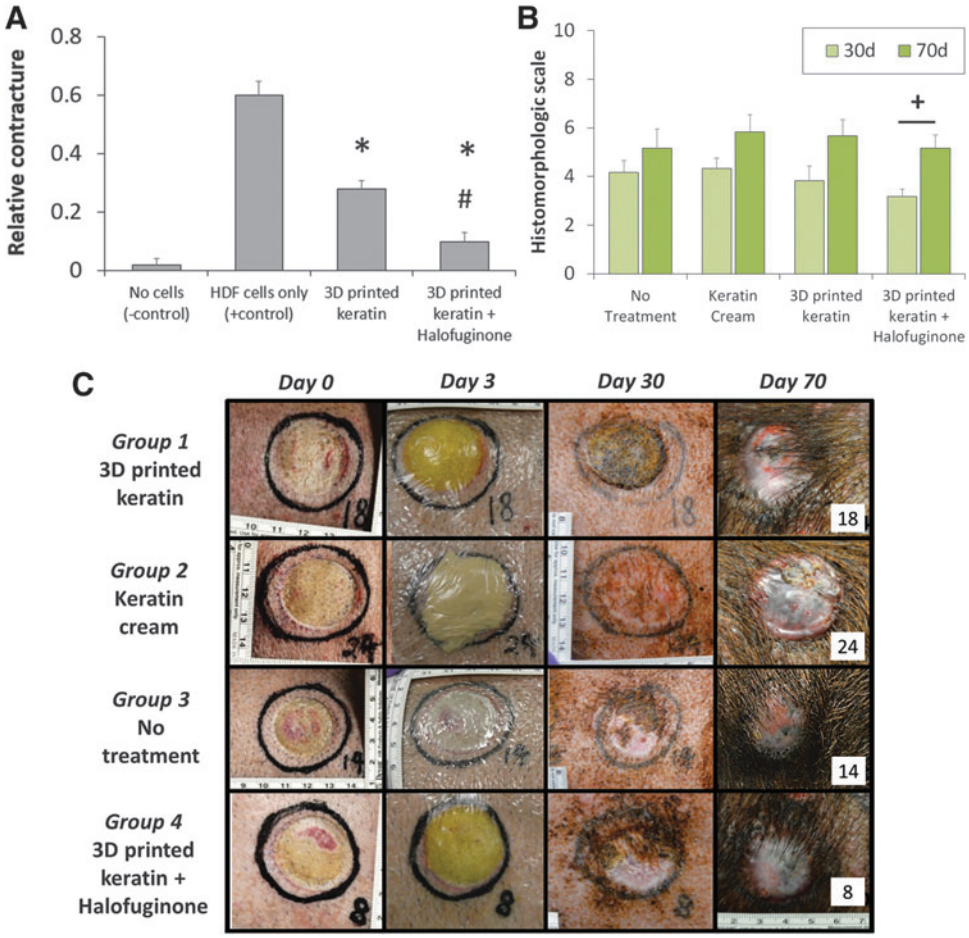

FIG. 2. **(A)** *In vitro* contracture assay using a cell-laden collagen gel treated with loaded or unloaded keratin hydrogels. The use of 3D printed keratin constructs was generally positive to reduce relative contracture compared with no treatment group; the inclusion of Halofuginone further reduces contracture. Statistical significance: *difference when compared with HDF cells only group, $p < 0.01$; #difference when compared with 3D printed keratin group, $p < 0.01$. **(B)** Combined histomorphologic scores at 30 and 70 days post-implantation, expressed as average mean ± standard of error, best possible outcome = 10, worst = 0. Statistical significance: +mean histomorphologic score is different at days 30 and 70, $p < 0.001$. **(C)** Representative macroscopic images showing treatment groups at day 0 (burn induction), day 3 (initial treatment applications), day 30 and 70 (biopsy collection, end points). HDF, human dermal fibroblasts.

On a case closer to our own, Xu *et al.*[19] used freeze-dried keratin scaffolds on a Wistar rat model and reported less contraction compared with a nonscaffold treatment, additional to earlier vascularization, thicker epidermis, and hair follicle formation.[19] In this study, we further demonstrated that crosslinked keratin has a significant effect on contraction, either caused by products of keratinolysis being released into the medium or by the hydrogel soaking up a portion of the nutrients in the contracture media being used, resulting in decreased nutrient availability (and subsequent contracture potential) for the fibroblasts. Compared with literature, our data in this study confirms reported results for hydrogels, loaded or not, supporting reductions in contracture in dermal wounds. We further confirm studies and effects of Halofuginone and keratin use, although our studies are the first to report them coupled together. As collagen constructs reported previously, the 3D printed keratin does not inhibit the effect of the loaded component, in this case Halofuginone, and it provides an adequate transport system with the additional characteristic of controlled geometry for delivery to complex dermal wounds.

In vivo *assessments of keratin-based hydrogels*

The efficacy of Halofuginone-loaded scaffolds in healing dermal burn wounds was assessed *in vivo* using a swine burn model. Healing parameters studied included order of collagen microstructures, regrowth of dermal appendages, and lack of hyperkeratosis or hyperplasia, among others. Animal models to assess excessive dermal scarring include rabbit ear or porcine dermis.[57] Red Duroc pigs in particular are a suitable model for hypertrophic scarring and excessive contraction following cutaneous injury.[58,59] The objective of this study was to evaluate the ability of 3D printed keratin constructs loaded with Halofuginone to reduce burn-induced hypertrophic scarring and contracture in a porcine partial-thickness burn model.

Partial-thickness burns were created on the dorsum of a Red Duroc pig using a brass burn block, and wounds were dressed with 3D printed keratin constructs, unloaded or supplemented with Halofuginone, at day 3 postinjury. In the current study, we utilized a histomorphologic scale methodology[41] to determine the efficacy of the three different treatment groups (keratin-based formulations) in reducing burn-induced hypertrophic scarring and contracture versus no treatment (negative control). Injury to epithelial and mesenchymal dermal components was determined by examining the presence and/or absence of epithelial hyperplasia, epidermal hyperkeratosis, inflammation, vascular proliferation, and appendage structures, including hair follicles, apocrine glands, and smooth muscle, and scored as described in Table 1. Statistical histomorphologic findings are summarized in Figure 2B; individual time point results are shown as incidence formatted data (30 days in Table 2, and 70 days in Table 3) and as histologic images (30 days in Fig. 3 and 70 days in Fig. 4).

Table 2. Incidence of Histological Observation After 30 Days

Parameter examined	*Ideal*	*Group 1: 3D printed keratin*	*Group 2: keratin cream*	*Group 3: no treatment*	*Group 4: 3D printed keratin + Halofuginone*
Hyperkeratosis	Absent	1/6	4/6	1/6	1/6
Epidermal hyperplasia	Absent	0/6	0/6	0/6	0/6
Hair follicle	Present	6/6	5/6	6/6	4/6
Apocrine glands	Present	6/6	6/6	6/6	6/6
Smooth muscle	Present	0/6	2/6	3/6	2/6
Collagen orientation	Normal (+3)	0/6	0/6	0/6	0/6
	Abnormal (+2)	0/6	0/6	0/6	0/6
	Abnormal (+1)	5/6	6/6	6/6	5/6
Inflammation	Absent	1/6	2/6	3/6	2/6
Vascular proliferation	Absent	0/6	1/6	0/6	1/6

3D, three-dimensional.

Representative biopsy sections from each of the burn sites ($n = 24$ per time point) at the 30 days time point showed no statistically significant differences among treatment groups. As summarized in Figure 2B and Table 2, the mean histomorphologic scarring score of about +4 was given to Groups 2 (4.33 ± 0.42), 3 (4.17 ± 0.48) and 4 (3.83 ± 0.60) (keratin cream, no treatment, and 3D keratin unloaded, respectively), and slightly lower (3.17 ± 0.31) for Group 1 (3D Halo).

Using macroscopic (Fig. 2C) and microscopic histologic (Fig. 3) data, epidermal hyperplasia was observed in all groups, and the absence of hyperkeratosis occurred only once in Groups 1, 3, and 4 but with greater incidence (four of six wounds) in Group 2. The presence of mesenchymal structures (dermal appendages), such as hair follicles, apocrine glands, smooth muscle (arrector pili), and blood vessels occurred variably but with similar incidence in all groups and thus, no significant treatment effect between treatments, including the untreated control. Specifically, apocrine glands were observed with equal incidence six of six wounds in all treatment groups. Smooth muscle had variable incidence: three of six wounds for Group 3, two of six wounds for Groups 2 and 4, but not observed zero of six wounds in Group 1. Figure 3 at 30 days reveals an immature formation of collagen in the upper layers of the dermis, characterized by the pale purple stain of the collagen rather than with bright blue.

Additional evaluation of collagen alterations using Picrosirius Red-stained sections under polarized light revealed equivalent collagen fiber disorganization in all treatment groups, particularly in the lower reticular dermis, and thus all wounds received a low score of +1 (Fig. 5). Less frequently observed changes such as the absence of inflammation and vascular proliferation occurred with similar incidence in all groups regarding of the treatment. It is important to highlight that in skin wound healing, after 30 and 70 days of wounding there should be a lower amount of vessels sprouting in the dermis and none present in the epidermis, which is the normal anatomy of skin.[45] The growth of vessels, vascularization, should be rapid and appropriate after the scaffolds are implanted to ensure proper oxygen and nutrient delivery for healing and remodeling to occur.[45,51] At our later time points, the vascular network should have matured to a stable and efficient system. But increasing the amount of vascularization at such late stages could be indicative of the healing and remodeling processes still occurring. Overall, such late advancing vascularization could be indicative of suboptimal healing. The incidence of active chronic inflammation was similar in three groups: absent in three of six wounds for Group 3, in two of six wounds for Groups 2 and 4, but absent in one of six wounds for Group 1. Vascular proliferation was absent in one of six wounds for Groups 2 and 4, but present in six of six wounds for Groups 1 and 3.

At the 70-day time point, wound healing mostly continued the trends observed at 30 days, as summarized in Figure 2B and Table 3, and evaluation again showed no statistically significant differences among treatment groups. A mean score of about +5 was given to for Groups 1 (5.17 ± 0.54) and 3 (5.17 ± 0.79), and a score close to +6 for

Table 3. Incidence of Histological Observation After 70 Days

Parameter examined	*Ideal*	*Group 1: 3D printed keratin*	*Group 2: keratin cream*	*Group 3: no treatment*	*Group 4: 3D printed keratin + Halofuginone*
Hyperkeratosis	Absent	6/6	5/6	4/6	4/6
Epidermal hyperplasia	Absent	0/6	0/6	0/6	0/6
Hair follicle	Present	3/6	5/6	6/6	4/6
Apocrine glands	Present	5/6	5/6	6/6	6/6
Smooth muscle	Present	1/6	2/6	1/6	2/6
Collagen orientation	Normal (+3)	0/6	0/6	0/6	0/6
	Abnormal (+2)	2/6	4/6	2/6	4/6
	Abnormal (+1)	4/6	2/6	4/6	2/6
Inflammation	Absent	4/6	4/6	4/6	3/6
Vascular proliferation	Absent	4/6	4/6	2/6	3/6

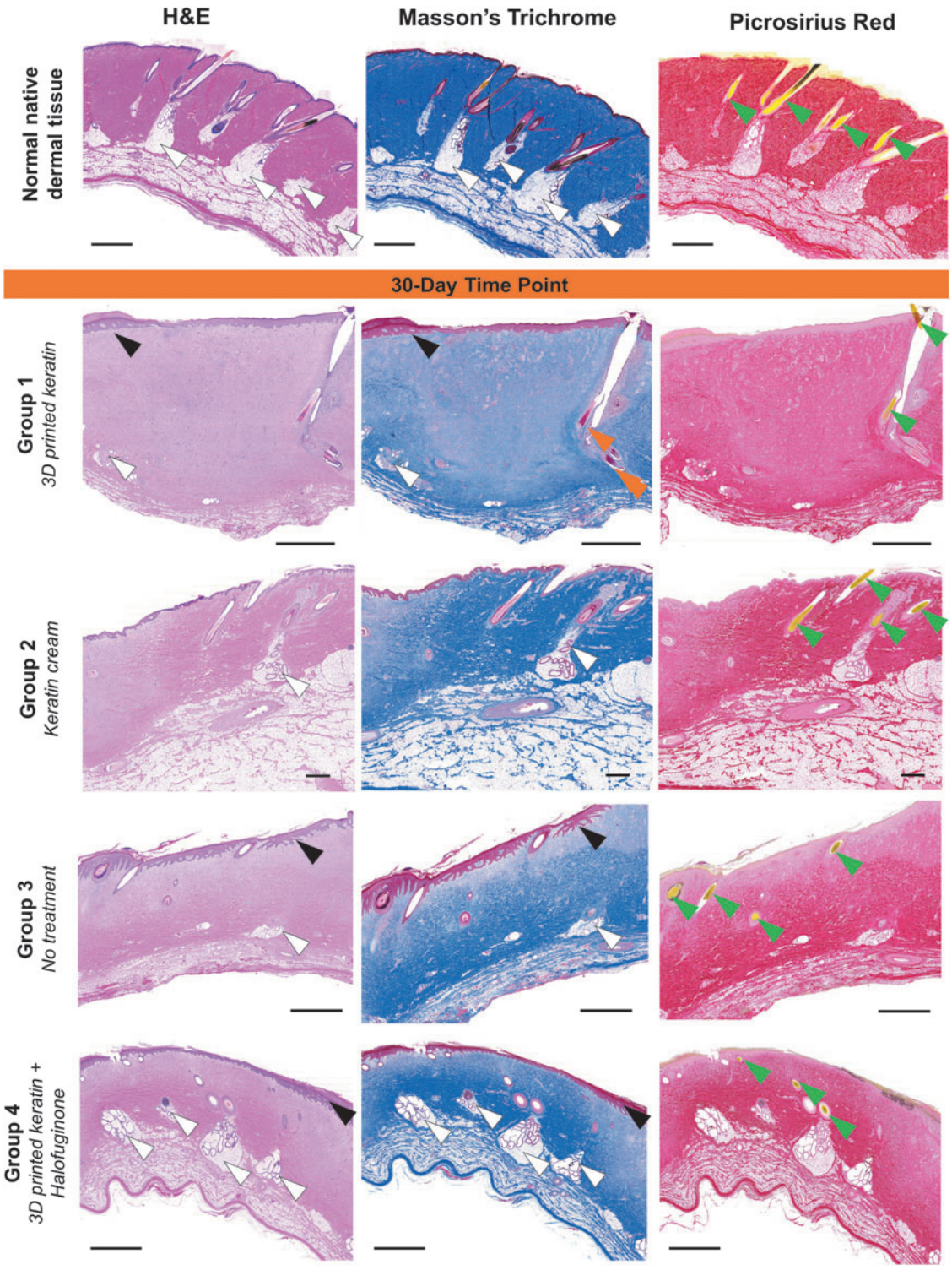

FIG. 3. Representative histological sections (H&E, Masson's Trichrome, and Picrosirius Red stains, 20× magnification) of all treatment groups after 30 days. At 30 days postprocedure, there are general cases of epidermal and dermal hyperplasia and hyperkeratosis (*black arrows*), and immature collagen deposition (comparison of vibrant stain in native tissue compared with *pale pink* by H&E, *pale blue* by Masson's Trichrome, and *pale red* by Picrosirius Red) predominantly involving the papillary dermis and upper reticular dermis. Dermal appendages such as hair follicles (*green arrowheads*), smooth muscle (*orange arrows*, confirmed with alpha smooth muscle actin, not shown), or glands (*white arrowheads*) appear in multiple cases. Scales: 2 mm. H&E, Hematoxylin and Eosin.

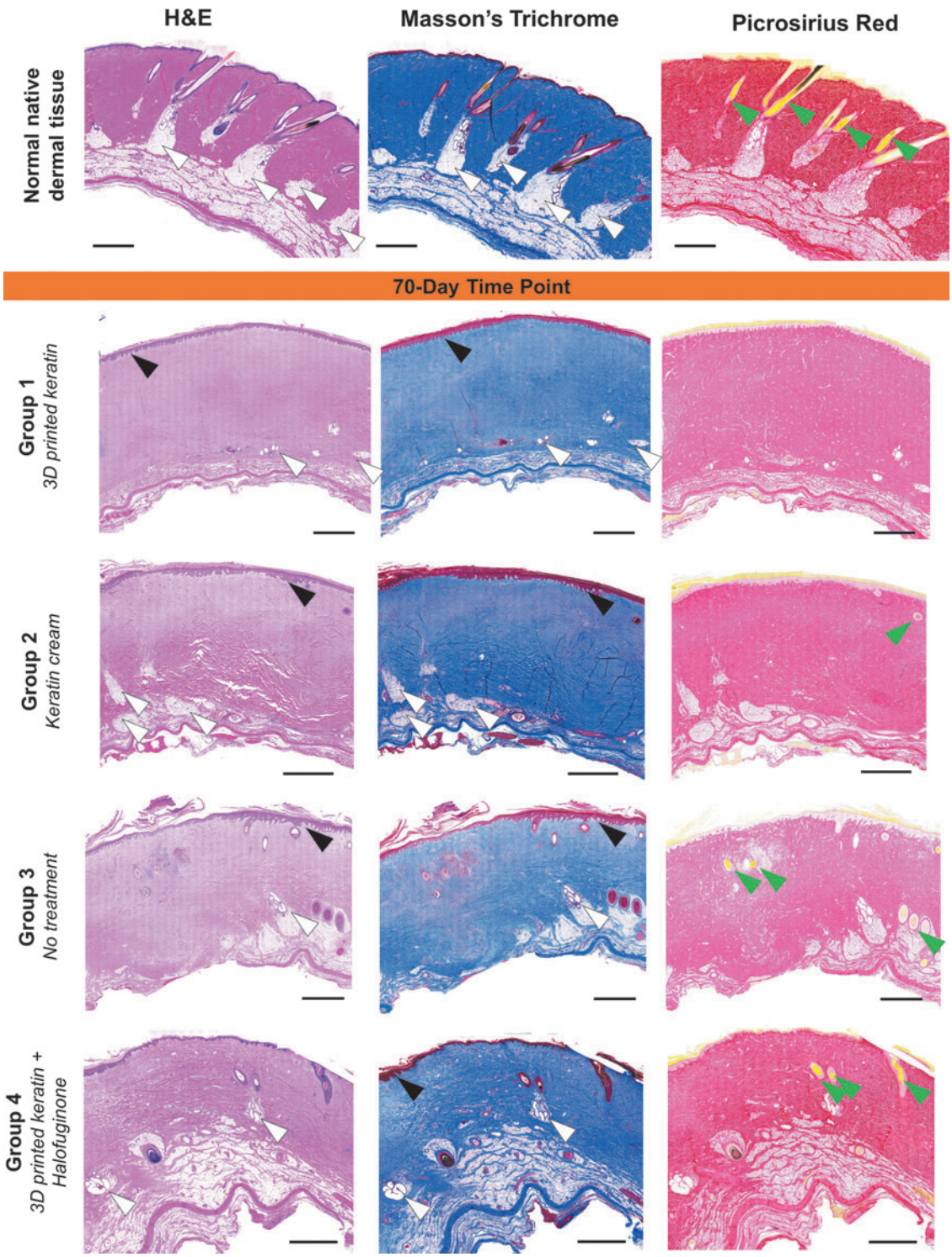

FIG. 4. Representative histological sections (H&E, Masson's Trichrome, and Picrosirius Red stains, 20×magnification) of all treatment groups after 70 days. At 70 days postprocedure, there are indications that for all groups the layers have matured, although the decrease of hyperplasia and hyperkeratosis (*black arrows*) is negatively compensated with an apparent decrease in the number of dermal appendages such as hair follicles (*green arrows*) or glands (*white arrows*). The collagen networks in all groups seem more homogeneous when compared with day 30 (Fig. 3), but do not present the organized, dense structure of native tissue (vibrant, dense coloration, compared with the treatments showing *pale pink* by H&E, *pale blue* by Masson's Trichrome, and *pale red* by Picrosirius Red). Scales: 2 mm.

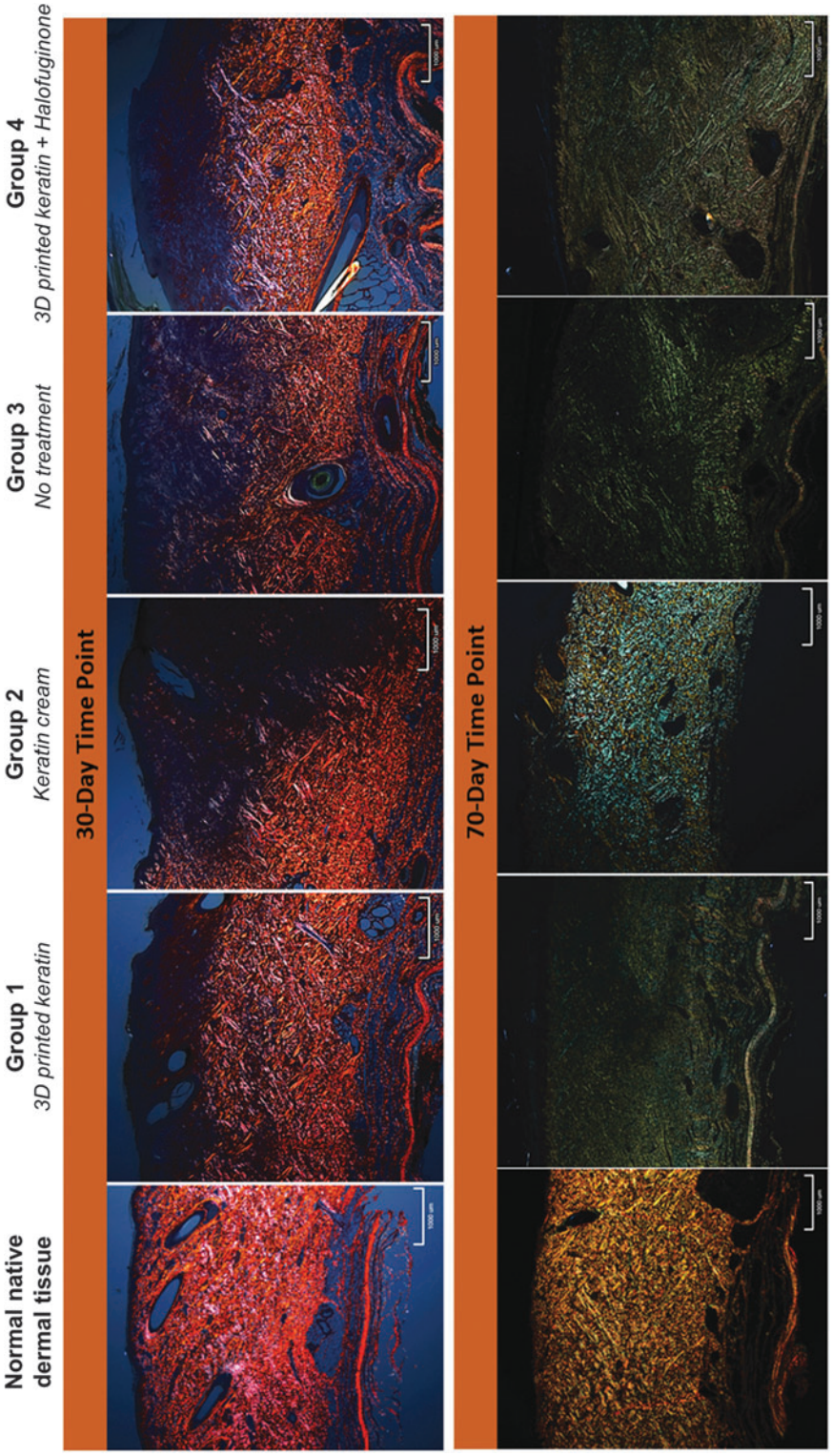

FIG. 5. Representative (low-power, ×20) sections of Picrosirius Red-stained samples of all treatment groups imaged under polarized light. Collagen content and order is characterized by the intensity and pattern of polarized light-induced birefringence of collagen fibers. Intense *red/orange/yellowish* birefringence indicates mature and organized collagen fibers (control, normal tissue, far left). *Green* birefringence has generally been correlated to immature, fine, and less organized collagen, although color change can be correlated to rotations of the samples and light incidence.[51] In this study, color was not considered to assess quality of the collagen but merely to identify it and its general orientation trends. At 30 days post-procedure, the heterogeneity of coloration is indication of collagen orienting in different directions (*black*, *purple*, *orange*, and *red* are indicative of different orientation); collagen is only present but disorganized in the lower reticular dermis. At 70 days, images show improved patterns or heterogeneity, with collagen present throughout the dermal layers although still disorganized with different orientations colored *blue/green* and *yellow*. Scale shown: 1 mm.

Groups 2 (5.83 ± 0.70) and 4 (5.67 ± 0.67). Using macroscopic (Fig. 2C) and microscopic (Fig. 4) information, we observed the absence of hyperkeratosis occurred with slightly variable incidence among all groups but with a positive trend favorable to Groups 1 and 2, although the scores for Groups 3 and 4 were not far behind. The presence of epidermal hyperplasia was a frequent finding as it occurred with equal incidence in all wounds regardless of treatment. However, the presence of normal appendage structures varied between groups without trend. Hair follicles were frequently observed with a variable incidence between treatment groups; in three of six wounds for Group 1, four of six wounds for Group 4, five of six wounds for Group 2, and six of six wounds for Group 3. The presence of apocrine glands occurred with equal incidence five of six wounds for Groups 1 and 2; and six of six wounds for

Groups 3 and 4, respectively. Similar findings were observed for the presence of smooth muscle, with equal incidence occurring in one of six wounds for Groups 1 and 3; and two of six wounds for Groups 2 and 4. Collagen fiber alterations appeared to have diminished in all groups but with best overall improvements observed in Groups 2 and 4 when compared with lower scores in Groups 1 and 3 (Figs. 4 and 5).

There was an improvement in the incidence of collagen, observed in the H&E, Masson's Trichrome, and Picrosirius Red stains, score of +2 assigned to Groups 2 and 4 in four of six wounds versus two of six wounds for Groups 1 and 3. A score of +2 is characterized by abnormal weave pattern of collagen only limited to the papillary dermis, having collagen throughout the cross-section of the samples. Again, while these changes (improvement in collagen organization) were not statistically significant between treatment groups at 70 days postprocedure, they may be considered favorable trends toward improving the outcome of burn-injury scarring. Other parameters examined, such as inflammation and vascular proliferation, showed similar histological findings between treatment groups, and thus, no statistical significance was found. The incidence of active chronic inflammation occurred equally in three groups; absent in four of six wounds for Groups 1, 2, and 3; and absent in three of six wounds for Group 4. Vascular proliferation occurred equally in two groups; absent in four of six wounds for Groups 1 and 2, but at lower incidence two and three of six wounds for Groups 3 and 4.

Most of the parameters examined appeared to have been improved over time when comparing the 30-day versus 70-day time points, except for the presence of epidermal hyperplasia, which was observed in all wounds regardless of the treatment and time points. However, the referenced overall improvements were not considered statistically significant. While the overall improvement in collagen organization observed between treatment groups by the 70-day endpoint was nonsignificant, there was general trend favorable to dressing wounds with keratin cream and 3D keratin unloaded that was demonstrated by the improvement in the level of collagen fiber organization. The most important improvement was the statistically significant difference in the total outcome scores for Group 1 (3D Halo) at 30 days (3.17 ± 0.31) versus at 70 days (5.17 ± 0.54) postprocedure (p-value $= 0.0094$). It is worth highlighting again that this group, the 3D printed keratin scaffolds loaded with Halofuginone, was the only sample to present significant improvement between days 30 and 70. This is indicative that the use of 3D printed keratin is not inhibiting the healing processes, and the inclusion of Halofuginone induces a more organized dermal healing after a burn; in other words, this treatment is slower but improves healing.

As a collagen inhibitor, the Halofuginone appears to initially delay collagen deposition, order, and general healing, which is then recovered at a later time point, although presenting no significant improvement when compared with the other groups at the 70-day endpoint of our study. This is supported by our previous *in vitro* observations on contracture and reports in literature. Three-dimensional printed keratin is noninferior to other reported natural, regenerative scaffolds for skin wounds *in vivo*,[19,52–56] and it includes the additional complex parameters of controlled geometry through 3D printing and drug delivery.

Last, it is important to comment on the limitations of the histomorphologic scale used in this study. This scale bundles all the scored parameters into a single number, and that value is not significantly different for all the treatments studied, including the no-treatment group (Fig. 2B). The scoring was based on similar published assessments to quantify cutaneous scarring,[41] but it would be important to highlight that all the parameters scored might not have the same value. For example, collagen organization scored higher for Groups 2 and 4 compared with the nontreatment case (Group 3), which is an important finding for proper wound healing, but this fact was obscured by the lack of significant difference between the histomorphologic scores of all groups. It would be possible to state that collagen organization has more value to wound healing than the appearance of hair follicles, but other questions might consider the absence of hyperplasia or inflammation with higher incidence in the final score.

Conclusions

Our previous studies on 3D printed keratin had given us indications that the scaffolds could be used as a drug delivery mechanism for the treatment of dermal burn wounds. In this study, we have further elucidated on the manufacturing process and the effects of critical steps such as lyophilization and sterilization. Keratin-based bioink can be used to produce large amounts of scaffolds for topical use on wounds, and we now have a better understanding of how 3D printed geometrical features, crosslinking properties, or mass are altered when the constructs undergo freeze-thawing cycles and gamma irradiation. We now have built a complete protocol to 3D print keratin scaffolds that can be used *in vivo*, including the presentation of a viable form of customized packing for production and transportation. Furthermore, keratin hydrogels are viable for the uptake and release of a contracture-inhibiting drug such as Halofuginone, which provides a mechanism to reduce scarring of severe burn wounds.

In vivo data show that the Halofuginone-laden printed keratin is noninferior to other similar approaches reported here in our study, and by others in literature. Although not entirely solving the issue of hyperplasia, this particular treatment does result in growth of apocrine glands and hair follicles, in the development of smooth muscle although to a lesser effect, it does provide an environment with low inflammation and low late-stage vascular proliferation, and a general improvement in collagen deposition and order over 70 days. The combined use of keratin and Halofuginone showed significant improvement in healing from days 30 to 70, compared with any other group studied, indicative of the inhibiting effect of Halofuginone on collagen deposition, which gives time to organization and healing.

Considering the limitations of the histomorphologic scoring, these studies are indicative of the potential of keratin bioink in delivering small molecules to support dermal wound healing. Having proven its viability *in vitro* and *in vivo*, in this and in previous studies,[8,38,39] we aim to keep increasing the complexity of the 3D printed constructs and exploring optimization alternatives, such as the ruthenium crosslinker or the order of Halofuginone loading in the manufacturing process, particularly aiming to treat complex facial burn wounds and elucidate in complex topographical reconstruction of dermal tissues.

Acknowledgments

The authors thank the Fulbright Scholars Program (J.N.), as well as the Department of Bioengineering's Fischell Fellowship (J.N.) at the University of Maryland.

Disclosure Statement

J.N. and J.P.F. declare no conflict of interest. This work was completed under collaboration with KeraNetics, LLC. R.M.C., R.C.H., A.R.G., G.J.H., and L.R.B. are employed by KeraNetics, LLC. R.J.C. is an employee of the United States government and has no financial interests in KeraNetics, LLC.

Author Contributions

J.N., R.M.C., R.C.H., A.R.G., G.J.H., R.J.C., L.R.B., and J.P.F. designed research; J.N., R.MC., R.C.H., and G.J.H. performed research; J.N., R.M.C., R.C.H., L.R.B., and J.P.F. analyzed data; and J.N., R.M.C., R.C.H., A.R.G., G.J.H., R.J.C., L.R.B., and J.P.F. wrote the article.

Funding Information

This material is based upon work supported by USAMRAA under Contract No. W81XWH-14-C-0022. Any opinions, findings and conclusions or recommendations expressed in this material are those of the author(s) and do not necessarily reflect the views of USAMRAA. This research was supported by the National Institute of Biomedical Imaging and Bioengineering/National Institutes of Health (NIBIB/NIH) Center for Engineering Complex Tissues (P41 EB023833).

Supplementary Material

Supplementary Data
Supplementary Figure S1

References

1. Wolf, S.E., Kauvar, D.S., Wade, C.E., *et al.* Comparison between civilian burns and combat burns from operation Iraqi freedom and operation enduring freedom. Ann Surg **243,** 786, 2006.
2. Rouse, J.G., and Van Dyke, M.E. A review of keratin-based biomaterials for biomedical applications. Materials (Basel) **3,** 999, 2010.
3. O'Brien, F.J. Biomaterials & scaffolds for tissue engineering. Mater Today **14,** 88, 2011.
4. Boateng, J.S., Matthews, K.H., Stevens, H.N., and Eccleston, G.M. Wound Healing dressings and drug delivery systems: a review. J Pharm Sci **97,** 2892, 2008.
5. Malafaya, P.B., Silva, G.A., and Reis, R.L. Natural-origin polymers as carriers and scaffolds for biomolecules and cell delivery in tissue engineering applications. Adv Drug Deliv Rev **59,** 207, 2007.
6. Nicodemus, G.D., and Bryant, S.J. Cell encapsulation in biodegradable hydrogels for tissue engineering applications. Tissue Eng Part B Rev **14,** 149, 2008.
7. Young, S., Wong, M., Tabata, Y., and Mikos, A.G. Gelatin as a delivery vehicle for the controlled release of bioactive molecules. J Control Release **109,** 256, 2005.
8. Placone, J.K., Navarro, J., Laslo, G.W., *et al.* Development and characterization of a 3D Printed, keratin-based hydrogel. Ann Biomed Eng **45,** 237, 2017.
9. Ham, T.R., Lee, R.T., Han, S., *et al.* Tunable keratin hydrogels for controlled erosion and growth factor delivery. Biomacromolecules **17,** 225, 2016.
10. Steinert, P.M., and Gullino, M.I. Bovine epidermal keratin filament assembly in vitro. Biochem Biophys Res Commun **70,** 221, 1976.
11. Thomas, H., Conrads, A., Phan, K.H., van de Löcht, M., and Zahn, H. In vitro reconstitution of wool intermediate filaments. Int J Biol Macromol **8,** 258, 1986.
12. Ikkai, F., and Naito, S. Dynamic light scattering and circular dichroism studies on heat-induced gelation of hard-keratin protein aqueous solutions. Biomacromolecules **3,** 482, 2002.
13. Sierpinski, P., Garrett, J., Ma, J., *et al.* The use of keratin biomaterials derived from human hair for the promotion of rapid regeneration of peripheral nerves. Biomaterials **29,** 118, 2008.
14. Pace, L.A., Plate, J.F., Smith, T.L. and Van Dyke, M.E. The effect of human hair keratin hydrogel on early cellular response tosciatic nerve injury in a rat model. Biomaterials **34,** 5907, 2013.
15. Pace, L.A., Plate, J.F., Mannava, S., *et al.* A human hair keratin hydrogel scaffold enhances median nerve regeneration in nonhuman primates: an electrophysiological and histological study. Tissue Eng Part A **20,** 131115063659000, 2013.
16. Tomblyn, S., Pettit Kneller, E.L., Walker, S.J., *et al.* Keratin hydrogel carrier system for simultaneous delivery of exogenous growth factors and muscle progenitor cells. J Biomed Mater Res Part B Appl Biomater **104,** 864, 2016.
17. Poranki, D., Whitener, W., Howse, S., *et al.* Evaluation of skin regeneration after burns in vivo and rescue of cells after thermal stress in vitro following treatment with a keratin biomaterial. J Biomater Appl **29,** 26, 2014.
18. Poranki, D.R., and Van Dyke, M.E. The effect of gamma keratose on cell viability invitro after thermal stress and the regulation of cell death pathway-specific gene expression. Biomaterials **35,** 4646, 2014.
19. Xu, S., Sang, L., Zhang, Y., Wang, X., and Li, X. Biological evaluation of human hair keratin scaffolds for skin wound repair and regeneration. Mater Sci Eng C **33,** 648, 2013.
20. Dias, G.J., Mahoney, P., Swain, M., *et al.* Keratin-hydroxyapatite composites: biocompatibility, osseointegration, and physical properties in an ovine model. J Biomed Mater Res Part A **95,** 1084, 2010.
21. Kowalczewski, C.J., Tomblyn, S., Wasnick, D.C., *et al.* Reduction of ectopic bone growth in critically-sized rat mandible defects by delivery of rhBMP-2 from kerateine biomaterials. Biomaterials **35,** 3220, 2014.
22. de Guzman, R.C., Saul, J.M., Ellenburg, M.D., *et al.* Bone regeneration with BMP-2 delivered from keratose scaffolds. Biomaterials **34,** 1644, 2013.
23. Humphries, J.D. Integrin ligands at a glance. J Cell Sci **119,** 3901, 2006.
24. Tachibana, A., Furuta, Y., Takeshima, H., Tanabe, T., and Yamauchi, K. Fabrication of wool keratin sponge scaffolds for long-term cell cultivation. J Biotechnol **93,** 165, 2002.
25. Verma, V., Verma, P., Ray, P., and Ray, A.R. Preparation of scaffolds from human hair proteins for tissue-engineering applications. Biomed Mater **3,** 025007, 2008.
26. Lin, C.-W., Yang, K.-C., Cheng, N.-C., *et al.* Evaluation of adhesion, proliferation, and differentiation of human adipose-derived stem cells on keratin. J Polym Res **25,** 40, 2018.
27. Han, S., Ham, T.R., Haque, S., Sparks, J.L., and Saul, J.M. Alkylation of human hair keratin for tunable hydrogel

erosion and drug delivery in tissue engineering applications. Acta Biomater **23,** 201, 2015.
28. Richter, J.R., de Guzman, R.C., and Van Dyke, M.E. Mechanisms of hepatocyte attachment to keratin biomaterials. Biomaterials **32,** 7555, 2011.
29. Wang, S., Wang, Z., Foo, S.E.M., *et al.* Culturing fibroblasts in 3D human hair keratin hydrogels. ACS Appl Mater Interfaces **7,** 5187, 2015.
30. Baker, H.B., Passipieri, J.A., Siriwardane, M., *et al.* Cell and growth factor-loaded keratin hydrogels for treatment of volumetric muscle loss in a mouse model. Tissue Eng Part A **23,** 572, 2017.
31. Passipieri, J.A., Baker, H.B., Siriwardane, M., *et al.* Keratin hydrogel enhances in vivo skeletal muscle function in a rat model of volumetric muscle loss. Tissue Eng Part A **23,** 556, 2017.
32. Saul, J.M., Ellenburg, M.D., De Guzman, R.C., and Dyke, M. Van. Keratin hydrogels support the sustained release of bioactive ciprofloxacin. J Biomed Mater Res Part A **98 A,** 544, 2011.
33. Pines, M., and Nagler, A. Halofuginone: a novel antifibrotic therapy. Gen Pharmacol Vasc Syst **30,** 445, 1998.
34. Luo, Y., Xie, X., Luo, D., Wang, Y., and Gao, Y. The role of halofuginone in fibrosis: more to be explored? J Leukoc Biol **102,** 1333, 2017.
35. Pines, M., Snyder, D., Yarkoni, S., and Nagler, A. Halofuginone to treat fibrosis in chronic graft-versus-host disease and scleroderma. Biol Blood Marrow Transplant **9,** 417, 2003.
36. Leiba, M. Halofuginone inhibits NF-kB and p38 MAPK in activated T cells. J Leukoc Biol **80,** 399, 2006.
37. Hill, P., Brantley, H., and Van Dyke, M. Some properties of keratin biomaterials: kerateines. Biomaterials **31,** 585, 2010.
38. Navarro, J., Swayambunathan, J., Lerman, M., Santoro, M., and Fisher, J.P. Development of keratin-based membranes for potential use in skin repair. Acta Biomater **83,** 177, 2019.
39. Navarro, J., Swayambunathan, J., Santoro, M., and Fisher, J. Assessment of the effects of energy density in crosslinking of keratin-based photo-sensitive resin. In: 2018 IX International Seminar of Biomedical Engineering (SIB), Bogotá, Colombia: IEEE, 2018.
40. de Guzman, R.C., Merrill, M.R., Richter, J.R., *et al.* Mechanical and biological properties of keratose biomaterials. Biomaterials **32,** 8205, 2011.
41. Singer, A.J., Thode, H.C., Jr., and McClain, S.A. Development of a histomorphologic scale to quantify cutaneous scars after burns. Acad Emerg Med **7,** 1083, 2000.
42. Balaji, S., Kumar, R., Sripriya, R., *et al.* Characterization of keratin-collagen 3D scaffold for biomedical applications. Polym Adv Technol **23,** 500, 2012.
43. Elvin, C.M., Vuocolo, T., Brownlee, A.G., *et al.* A highly elastic tissue sealant based on photopolymerised gelatin. Biomaterials **31,** 8323, 2010.
44. Sando, L., Kim, M., Colgrave, M.L., *et al.* Photochemical crosslinking of soluble wool keratins produces a mechanically stable biomaterial that supports cell adhesion and proliferation. J Biomed Mater Res Part A **95A,** 901, 2010.
45. Markeson, D., Pleat, J.M., Sharpe, J.R., *et al.* Scarring, stem cells, scaffolds and skin repair. J Tissue Eng Regen Med **9,** 649, 2015.
46. Tyan, Y.-C., Liao, J.-D., Lin, S.-P., and Chen, C.-C. The study of the sterilization effect of gamma ray irradiation of immobilized collagen polypropylene nonwoven fabric surfaces. J Biomed Mater Res **67A,** 1033, 2003.
47. Escudero-Castellanos, A., Ocampo-García, B.E., Domínguez-García, M.V., Flores-Estrada, J., and Flores-Merino, M.V. Hydrogels based on poly(ethylene glycol) as scaffolds for tissue engineering application: biocompatibility assessment and effect of the sterilization process. J Mater Sci Mater Med **27,** 176, 2016.
48. Kanjickal, D., Lopina, S., Evancho-Chapman, M.M., Schmidt, S., and Donovan, D. Effects of sterilization on poly(ethylene glycol) hydrogels. J Biomed Mater Res Part A **87A,** 608, 2008.
49. Hodder, E., Duin, S., Kilian, D., *et al.* Investigating the effect of sterilisation methods on the physical properties and cytocompatibility of methyl cellulose used in combination with alginate for 3D-bioplotting of chondrocytes. J Mater Sci Mater Med **30,** 10, 2019.
50. Hu, M.S., Maan, Z.N., Wu, J.-C., *et al.* Tissue engineering and regenerative repair in wound healing. Ann Biomed Eng **42,** 1494, 2014.
51. Böttcher-Haberzeth, S., Biedermann, T., and Reichmann, E. Tissue engineering of skin. Burns **36,** 450, 2010.
52. Metcalfe, A.D., and Ferguson, M.W.J. Bioengineering skin using mechanisms of regeneration and repair. Biomaterials **28,** 5100, 2007.
53. Zhong, S.P., Zhang, Y.Z., and Lim, C.T. Tissue scaffolds for skin wound healing and dermal reconstruction. Wiley Interdiscip Rev Nanomed Nanobiotechnol **2,** 510, 2010.
54. Powell, H.M., and Boyce, S.T. Wound closure with EDC cross-linked cultured skin substitutes grafted to athymic mice. Biomaterials **28,** 1084, 2007.
55. Powell, H., Supp, D., and Boyce, S. Influence of electrospun collagen on wound contraction of engineered skin substitutes. Biomaterials **29,** 834, 2008.
56. Ono, I., Tateshita, T., and Inoue, M. Effects of a collagen matrix containing basic fibroblast growth factor on wound contraction. J Biomed Mater Res **48,** 621, 1999.
57. Morris, D.E., Wu, L., Zhao, L.L., *et al.* Acute and chronic animal models for excessive dermal scarring: quantitative studies. Plast Reconstr Surg **100,** 674, 1997.
58. Gallant, C.L., Olson, M.E., and Hart, D.A. Molecular, histologic, and gross phenotype of skin wound healing in red Duroc pigs reveals an abnormal healing phenotype of hypercontracted, hyperpigmented scarring. Wound Repair Regen **12,** 305, 2004.
59. Harunari, N., Zhu, K.Q., Armendariz, R.T., *et al.* Histology of the thick scar on the female, red Duroc pig: final similarities to human hypertrophic scar. Burns **32,** 669, 2006.

Address correspondence to:
John P. Fisher, PhD
Fischell Department of Bioengineering
University of Maryland
4102A Clark Hall, 8278 Paint Branch Drive
College Park, MD 20742

E-mail: jpfisher@umd.edu

Received: July 15, 2019
Accepted: November 4, 2019
Online Publication Date: January 9, 2020